Available online at www.sciencedirect.com

SciVerse ScienceDirect

Journal of the European Ceramic Society 32 (2012) 2025–2034

www.elsevier.com/locate/jeurceramsoc

Characterization of microstructure and thermal properties of $Gd_2Zr_2O_7$-type thermal barrier coating

G. Moskal [a,*], L. Swadźba [a], M. Hetmańczyk [a], B. Witala [a], B. Mendala [a], J. Mendala [b], P. Sosnowy [c]

[a] *Silesian University of Technology, Department of Materials Science, Poland*
[b] *Silesian University of Technology, Department of Materials Technology, Poland*
[c] *Factory of Transport Equipment WSK "PZL – Rzeszów" Stock Company, Poland*

Available online 9 January 2012

Abstract

We present herein a characterization of the microstructure and thermal properties of thermal barrier coatings (TBCs), which we obtained via plasma spraying of powder $Gd_2Zr_2O_7$. By using X-ray diffraction (XRD) and electron backscatter diffraction (EBSD), we evaluated the phase composition of a ceramic layer and estimated the ceramic-layer stress state by the $\sin^2\psi$ method. The tests revealed that the TBC layer consisted of a single-phase structure of $Gd_2Zr_2O_7$, namely, an Fd3m lattice. The thermal diffusivity of the outer ceramic layer was determined based on a bilayer model and corrected with a factor to account for the presence of pores. The results reveal that the use of the standard parameters in a standard spraying process gives good-quality $Gd_2Zr_2O_7$ TBCs with a thermal conductivity considerably lower than 8YSZ-type TBCs.

Keywords: TBC; Zirconates; Thermal conductivity; Microstructure characterization

1. Introduction

Currently, the possibilities are very limited for further high-temperature applications (i.e., above 1200 °C) of thermal barrier coatings (TBC) with conventional outer ceramic $ZrO_2 \times 8Y_2O_3$ layers. On the one hand, this situation is due to the insurmountable barrier of the melting point of nickel superalloys, which are critical materials in the hot sections of gas turbines. On the other hand, the durability of ceramic TBCs is a difficult problem because their degradation rate increases at these temperatures.[1–6] Further modifications of the TBC structure (e.g., gradient coatings with YSZ) and of the chemical composition of the base ceramics (e.g., modification of the ZrO_2 oxide with RE_2O_3 rare earth oxides) has only a limited potential for increasing the outlet-gas temperature. To advance in this area, we must apply new types of ceramic materials with properties superior to those of the standard material (8YSZ). Such materials include those with a thermal conductivity coefficient that is smaller than that of 8YSZ.[7–11]

Thus, increasing the working temperature of gas turbines elements requires applying a new type of TBC—one with a coefficient of thermal conductivity below that of the $ZrO_2 \times 8Y_2O_3$ oxides. Such a material would lead not only to an increase in the lifetime of critical engine elements (e.g., combustion chambers), but also to an increase in turbine operating temperatures. The most effective approach to meet this need appears to be the use of low-thermal-conductivity materials of type $RE_2Zr_2O_7$ (where RE indicates a reactive element) for the outer ceramic layer. The consequences would be reduced temperatures in the insulated working areas with the concomitant decrease in oxidation kinetics within the bondcoat and in the generation of thermally grown oxides (TGOs), which are a determinant factor for the lifetime of TBC systems.[12–17]

The most important role of TBCs is to reduce the temperature of the metallic base in a stable manner and to thereby promote safe and long-lasting operations. This goal is achievable for an Al base by using (i) an effective insulating barrier in the form of a thin ceramic layer with a low thermal conductivity coefficient and thermal–chemical stability in the working atmosphere and (ii) an bondcoat material in the TGO zone. The thermal conductivity of these materials, which may be expressed by a thermal conductivity coefficient or by the thermal diffusivity, is a fundamental factor that determines if the charge materials (i.e., powders thermally sprayed onto the outer ceramic layer of the TBC) are appropriate. Thermal conductivity depends on the efficiency with which the material scatters phonons at structural

* Corresponding author.
E-mail address: grzegorz.moskal@polsl.pl (G. Moskal).

0955-2219/$ – see front matter © 2011 Elsevier Ltd. All rights reserved.
doi:10.1016/j.jeurceramsoc.2011.11.043

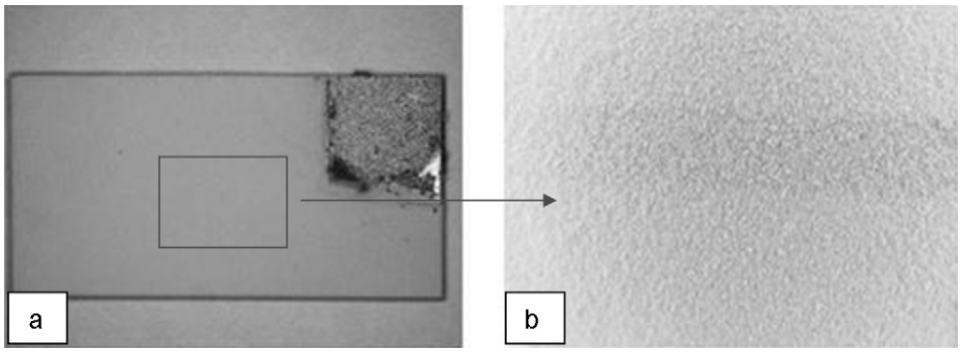

Fig. 1. General view of the $Gd_2Zr_2O_7$ TBC layer (a) and details of the surface that are visible with 32× stereoscope macroscope magnification (b).

defects (e.g., vacancies, foreign atoms, grain boundaries, etc.), which translates into a reduced mean-free path for phonons. However, the inner structure of the ceramic layer (i.e., the architecture of cracks and pores) deposited by the spraying process influences the thermal conductivity. Voids that are insulated from other artifacts are particularly important because they determine the effectiveness of a thermal insulation.[18–20]

2. Experimental procedure

In this study, we evaluated the microstructure and thermal properties of a TBC layer deposited by plasma spraying a ceramic powder with chemical composition $Gd_2Zr_2O_7$. This TBC was sprayed over a nickel AMS5599 superalloy precoated with a sprayed-on NiCrAlY interlayer. The base alloy was 2 mm thick and the NiCrAlY bondcoat was approximately 125 μm thick. A bondcoat and an outer ceramic layer were then sprayed over by APS with standard parameters.

The microstructure and technological and thermal properties of the base powder and ceramic powder are characterized in detail elsewhere.[21–23] Briefly, these characterizations include the following:

1. Visual inspection of outer surface of flat sprayed samples.
2. Macroscopic surface tests via stereoscope microscopy (SZX9, Olympus) with a magnification from 6.3× to 40×).
3. Topography measurements of outer ceramic layer with an analysis of the geometrical surface parameters (MicroProf contactless optical profilometer, Fries Research and Technology GmbH).
4. Surface evaluation by scanning electron microscopy (SEM, Hitachi model S-3400N).
5. Definition of phase composition and estimation of ceramic-layer stress state by the $\sin^2 \Psi$ method with the JEOL JDX-7S Roentgen diffraction instrument and electron backscatter diffraction (EBSD) detection (coupled with the Hitachi SEM).
6. Evaluation of TBC microstructure together with the characterization of its thickness and the quantity and quality of porosity. These measurements were done with an optical microscope (Olympus DP70) and a field-emission scanning electron microscope (FE-SEM, Hitachi S-4200) with cold field emission. The quality and quantity evaluations were done with in-house software that automatically analyzed the "MetIlo" image (J. Szala, Silesian University of Technology).
7. Microanalysis of chemical composition done via energy dispersive spectrometry (EDS) piloted by software produced by the Thermo Scientific System Seven Company (Hitachi S-4200).
8. Laser-flash (LF) thermal diffusivity tests of the TBC providing a direct measurement of the thermal diffusivity (model LFA 427, Netzsch). These measurements were done in a temperature range from 20 to 1100 °C in an argon atmosphere on $10 \times 10 \times 2\,mm^3$ samples. Layered materials consisting of the base, base + bondcoat, and base + bondcoat + outer ceramic layer were all tested. Cowan's model was used to determine the thermal diffusivity of the whole TBC system. Next, a bilayer model was used to determine the interlayer thermal diffusivity (at the known thermal diffusivity of the AMS5599 base material). A bilayer model was also used to determine the ceramic-layer thermal diffusivity with the thermal diffusivity of base plus bilayer serving as a reference.
9. Determination of the coefficient of thermal diffusivity of charge powders as a function of temperature. The determination was based on measurements of thermal diffusivity and known values of specific heat and coefficient of linear extension.[21–23]

3. Results and discussion

The first stage of measurements involved visual evaluation of samples with TBCs. The TBCs, which were based on the $Gd_2Zr_2O_7$ phase, were plasma sprayed onto the samples. The purpose of these measurements was to determine the macroscopic quality of the resulting layers. We particularly concentrated on the homogeneity in layer thickness and controlled for the possible presence of shoulders, delaminations, or cracks. These controls were done, for example, during measurements with the stereoscope microscope. Typical results of these macroscopic tests for the $Gd_2Zr_2O_7$ TBC layer are presented in Fig. 1. The macroscopic visual inspection revealed a good quality layer both in its core and within the sample area. The dark uncoated area of the sample is where it was held during the plasma-spraying process [Fig. 1(a)]. Visual inspection revealed no visible defects such as shoulders, delaminations, or cracks that would indicate an incorrect plasma-spraying process. The

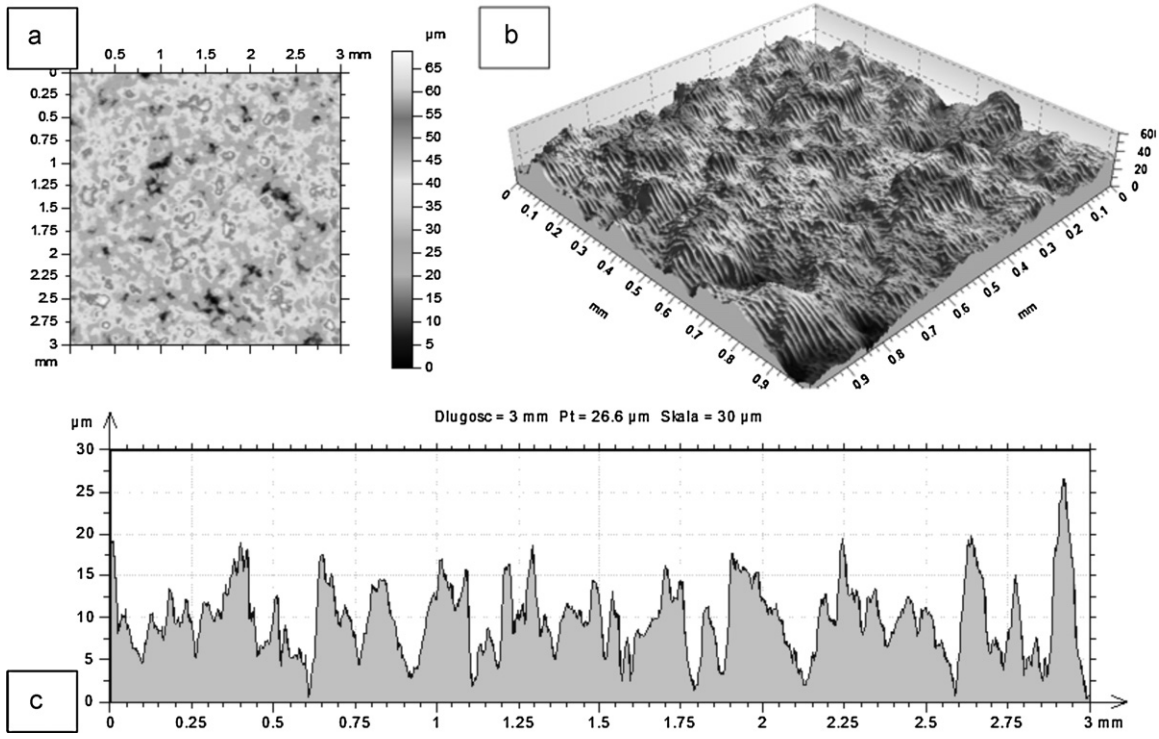

Fig. 2. Geometrical shape of surface of $Gd_2Zr_2O_7$ TBC layer in the form of (a) 2D isometric image of surface, (b) 3D topography of surface, and (c) roughness profile.

surface of the outer ceramic layer is characterized by roughness, which is obtained by the APS method [Fig. 1(b)].

To improve on the visual evaluation and produce a more detailed characterization, we used a contactless optical profilometer to describe the surface topography and evaluated the numerous parameters that characterize the ceramic-layer state. Fig. 2(a) and (c) shows the geometrical shape of a selected fragment of a tested surface ($1.0 \times 1.0\,mm^2$) in the form of an isometric two-dimensional (2D) image, a three-dimensional (3D) surface topography, and a roughness profile, respectively. We conclude from the surface maps, which quantitatively describes the surface geometry that the evaluated $Gd_2Zr_2O_7$ layer is characterized by a structure, typical for ceramic layers, which results from plasma spraying. We measured randomly selected areas including central zones and zones near the sample edges. The quantitative results for the geometrical parameters reveal no significant differences, which agree with the homogenous structure found in the macroscopic measurements. These quantitative results, which characterize the ceramic-layer surface geometry, are presented in Table 1.

The topography and surface roughness of a ceramic layer only partially characterize the real state of a sprayed surface. Although these measurements characterize in a precise quantitative manner some effects of the plasma-spraying process of ceramic powder and also provide information on the average state of the surface, they do not give detailed information regarding layer quality. Thus, a more in-depth evaluation of the layer morphology is essential and must consider the presence and structure of cracks, which are perpendicular to the base surface and form a lattice. A typical SEM image (Fig. 3) shows the surface of the topmost $Gd_2Zr_2O_7$ ceramic layer. The $Gd_2Zr_2O_7$ TBC is characterized by a structure that is typical for plasma-sprayed ceramic powders [Fig. 3(a)]. We observe "droplets," which are particles of powder congealed on the sprayed surface. The flattened shape of the droplets is the result the impact of the liquid drop on the solid ceramic phase. This system of congealed drops forms the TBC layers, which are lamellar in structure [Fig. 3(b)].

The very fast congealing of the ceramic material generates strong stresses in the ceramic layer, which manifests itself by a loss of coherence and a tendency for cracking in a lattice pattern.

Next, by using the XRD and EBSD techniques, we studied the phase composition of the outer ceramic layer. These methods allowed us to assess the phase composition in micro-areas; the results are presented in Fig. 4.

The "macro" assessment (by XRD) and micro assessment of phase composition revealed the single-phase nature of the $Gd_2Zr_2O_7$ layer with a pyrochlore (Fd3m) lattice, which is a

Table 1
Quantitative results for roughness of $Gd_2Zr_2O_7$ TBC layers. Rz is the maximum height of the roughness profile, Ra is the mean arithmetic deviation in roughness, and Rq is the mean square deviation in roughness.

	Left edge	Core I	Core II	Right edge
Rz [μm]	34.20	36.14	35.00	34.76
Ra [μm]	7.92	6.94	6.52	6.23
Rq [μm]	9.16	8.72	8.12	7.92

Rz, max height of profile of roughness; Ra, mean arithmetic deviation of profile of roughness; Rq, mean square deviation of profile of roughness.

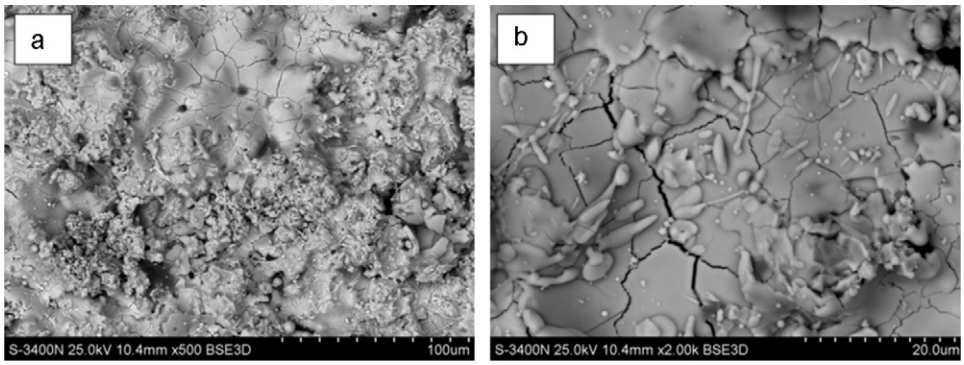

Fig. 3. Surface morphology of TBC $Gd_2Zr_2O_7$layers. (a) General view of a ceramic layer. (b) Details of surface showing droplets and lattice of cracks.

very advantageous phenomenon (considering the fact that the powder in its initial state is characterized by the presence of gadolinium oxides and zirconium oxide [24]). The single-phase nature of this layer, which results from plasma spraying, is also an extraordinarily essential feature because it leads to the conclusion of negligible influence of possible phase transformations on TBC lifetime under high-temperature operations.

The XRD tests also allowed us to evaluate the stresses that occur in a ceramic layer. Three fundamental factors influence the residual stresses in the TBC layers[25–27]:

1. Stress related to variations in the lattice dimensions of component phases of the TBC layers.
2. Stress that result from intense cooling of liquid drops in sprayed ceramic material.
3. Stress resulting from differences in the thermal coefficient of linear extension between a ceramic layer and a prime layer or base material.

The total stress in the TBCs is a sum of these three components (note that stress resulting from possible phase changes

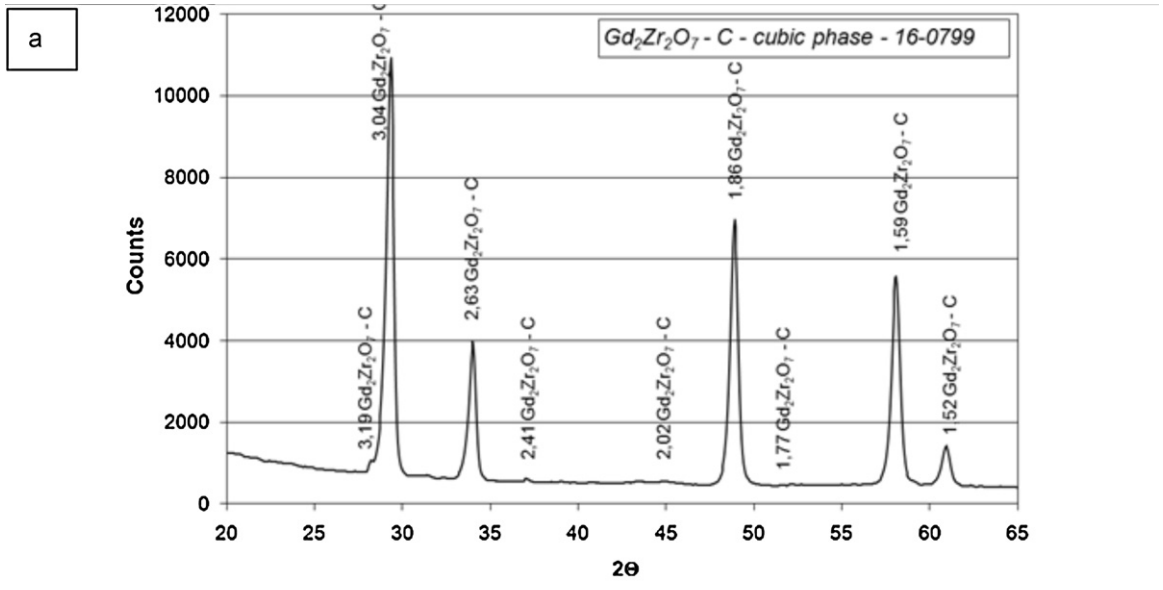

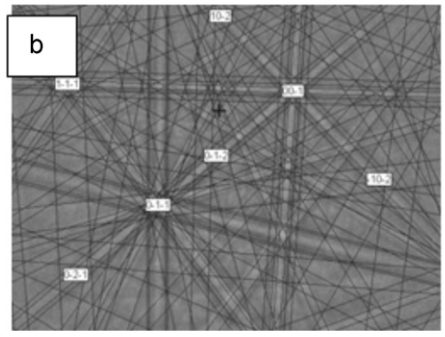

Name:	$Zr_2Gd_2O_7$
Laue and space group no.:	11,m3m,225
Unit cell lengths:	5.26, 5.26, 5.26Å
Unit cell angles:	90.0, 90.0, 90.0 °
Composition:	O (63.3), Zr (18.2), Gd (18,2) at %
Orientation:	76.3, 40.9, 29.6 °
Space plane:	(25-4)
MAD:	0,195

Fig. 4. XRD and EBSD results giving phase composition of $Gd_2Zr_2O_7$ layer.

Table 2
Thickness of a prime layer and a ceramic layer in the TBC system.

Thickness [μm]	NiCrAlY	$Gd_2Zr_2O_7$
Mean value	125	190
Max value	156	227
Min value	110	174
Standard deviation	7	6

Table 3
Characteristics of architecture of cracks and pores for TBC layer.

	$Gd_2Zr_2O_7$
Total porosity [%]	4.69
Participation of vertical pores [%]	0.18
Participation of horizontal pores [%]	1.79
Participation of spherical pores [%]	2.73
Mean length of horizontal pores [μm]	7.78
Mean thickness of horizontal pores [μm]	2.78
Value of ratio of length to thickness of horizontal pores	2.80

is considered to be negligibly small [26]). Moreover, a certain level of stress in the sandy base material is essential and was given in Ref.[25] to be 200 MPa and to be compressive. A lot of data are available in the literature regarding stress in TBC layers, but these data are very widely scattered because they depend on the measurement method, the type of sprayed layer, and the layer microstructure. Nevertheless, the most prevalent results for stress in TBC coatings directly after plasma spraying fall within 20 to 50 MPa and, depending on the publication, the stress may be either compressive or tensile. For these measurements, the ceramic-layer thickness was also essential.[28–35] In the present case, we estimate the stress by the $\sin^2\psi$ method to be −15 MPa.

This parameter is extraordinary essential from a point of view of durability of the TBC layers. Stresses resulting from the mismatch of linear extension coefficients and oxidation tend to form a TGO zone, which works to separate the base from the ceramic layer. Additional stresses result from creeping and plastic strains. All these stresses have strong influence on this parameter.[36]

Thickness is a fundamental parameter for thermally sprayed layers, including TBCs. In the present case, we have flat samples, so we measured the relevant thickness in randomly selected areas. Considering the stochastic nature of thermal spraying for coatings of this type, we expect a certain scatter in the results, which is expressed by the minimum and maximum thicknesses and the standard deviation. The results, which characterize the thickness of the NiCrAlY bondcoat and the $Gd_2Zr_2O_7$ ceramic layer, are presented in Table 2, and a general view of the spray-applied TBC is shown in Fig. 5. Because layer thickness depends on the parameters of the spraying process, the thickness may be a priori determined. In a case of TBC layers, the thickness of each layer usually does not exceed 300 μm. This limit results from the fact stresses in ceramic layers change with increasing in thickness, a state of stresses in a ceramic layer changes consequently, while in a case of thick layers, a value adopts positive values, what is equivalent to tensile stresses. Under normal operating conditions, this effect can shorten the lifetime of such systems unless the ceramic-layer porosity is increased.

The porosity of a ceramic layer is the next, very essential, parameter to analyze and is usually defined in terms of the quantity of participating pores and the presence of so-called mass porosity, which is a very unfavorable phenomenon. However, current design techniques based on mathematical modeling emphasize the microstructure of ceramic layers and, in particular, their thermal insulation capacity and the detailed characteristics of the so-called architecture of cracks and pores. From the quantitative and qualitative characteristics of voids that are present in the microstructure, it is possible to precisely model heat-transport phenomena and thereby to define the optimal parameters for the spraying process.

The characteristics of the architecture of analyzed voids are presented in Table 3. Pore participation does not exceed 6% total porosity, and the participation of individual types of pores is fairly homogeneous. The quantitative and qualitative characteristics of pores demonstrate a predominant participation of spherical and horizontal pores, which is favorable to improve the thermal properties of a layer. The participation of vertical pores is negligibly small. The values given in Table 3 are typical of ceramic layers that are plasma sprayed with standard spraying parameters, as may be confirmed by comparing with published results for TBC 8YSZ layers (see, e.g., Ref. [37]). However, no data is available for layers based on the $Gd_2Zr_2O_7$ phase. An analysis of the microstructure also revealed the presence of sample regions characterized by mass porosity. A view of the $Gd_2Zr_2O_7$ layer is presented in Fig. 6.

As for porosity, other TBC-layer microstructure elements that require evaluation (i.e., concerning a ceramic layer and a prime NiCrAlY layer as well) can be taken as correct. An analysis of the structure of the TBC system within the area in contact with the metallic base did not reveal any delaminations, impurities, or other artifacts due to the surface-preparation process. Within the bondcoat itself, no cracks were apparent and its structure was typical for the vacuum plasma spraying (VPS) method for MCrAlY powder. There are no visible indications that oxidation of the bondcoat occurs during the spraying process. In addition, the structure of the ceramic layer is also correct. Single spherically shaped spores are visible and interlamellar cracks, which developed as the flattened drops of the ceramic phase cooled, are also visible. The typical microstructure is presented in Fig. 7.

An analysis of the surface distribution of fundamental components indicates a new type of TBC layers has formed. Phase-composition tests (not included in this paper) demonstrated that the prime layer consists of nickel-rich phases [Ni(Cr) and Ni_3Al]. This layer contains particles of Al_2O_3 oxides that were created in the core of the layer during the spraying process; however, they can also occur locally on the surface of an interlayer. Typical distributions are presented in Fig. 8. A detailed image of the microstructure, particularly within the interlayer zone between the ceramic layer and the prime layer, did not reveal the presence of oxides in the TGO zone, which may be attributed to the high temperature during the thermal-spraying

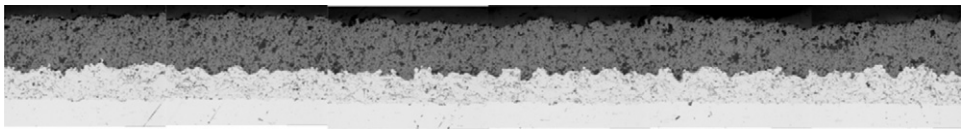

Fig. 5. General view of TBC $Gd_2Zr_2O_7$layers.

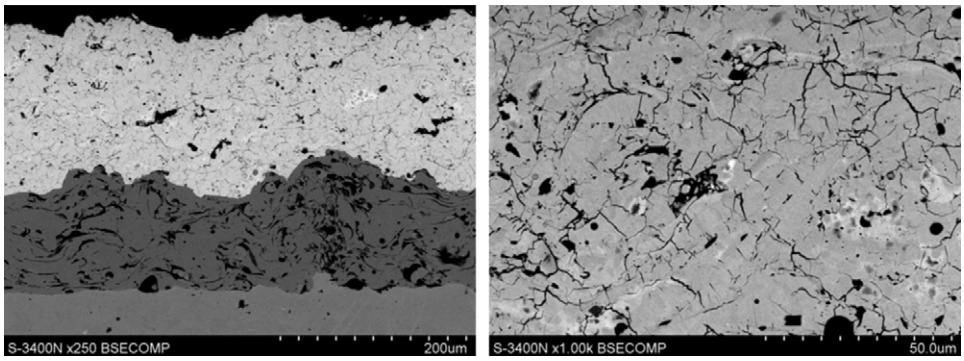

Fig. 6. $Gd_2Zr_2O_7$ ceramic layer with visible pores and cracks.

process. This question is one of the most essential problems in the research of TBC layers. Typical images of microstructure for this zone are shown in Fig. 9.

For TBC deposited by plasma spraying, the typical microstructure consists of particles remelted in the plasma and of ceramic particles that flatten when they hit the sample surface as a result of the energy acquired in an arch. A typical microstructure is presented in Fig. 7. Thus, the system consists of flattened particles oriented parallel to the base, of interparticle voids orientated perpendicular to the direction of heat flow, and of interparticle cracks that form perpendicular to the base when the sprayed particles cool. Moreover, the microstructure contains pores of different shapes and sizes. These microstructural features of the ceramic layers result in a low single-level thermal conductivity of approximately 1 W/mK. Note that this effect is related only to a geometrical component (thickness) and to the volume participation of pores and cracks. From the point of view of mechanical properties, these microstructural properties lead to a low rigidity ($E = 20$ GPa) and to a reduction in stress, which are consequences of a cyclic change of temperature and the differences in linear extension between base and coating.[38]

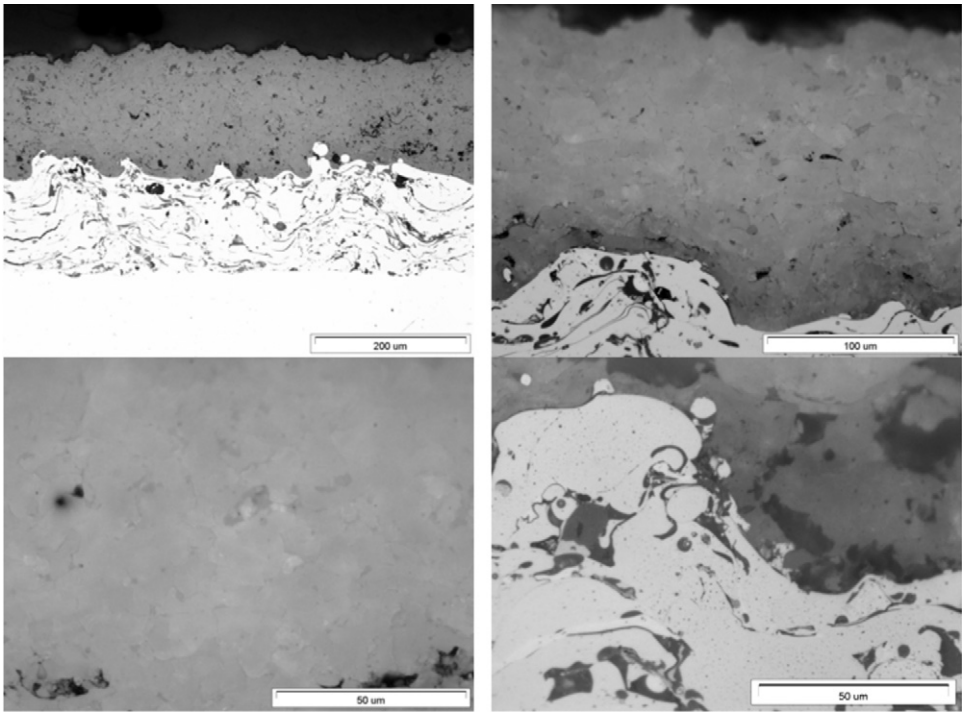

Fig. 7. Details of inner structure of TBC $Gd_2Zr_2O_7$layer.

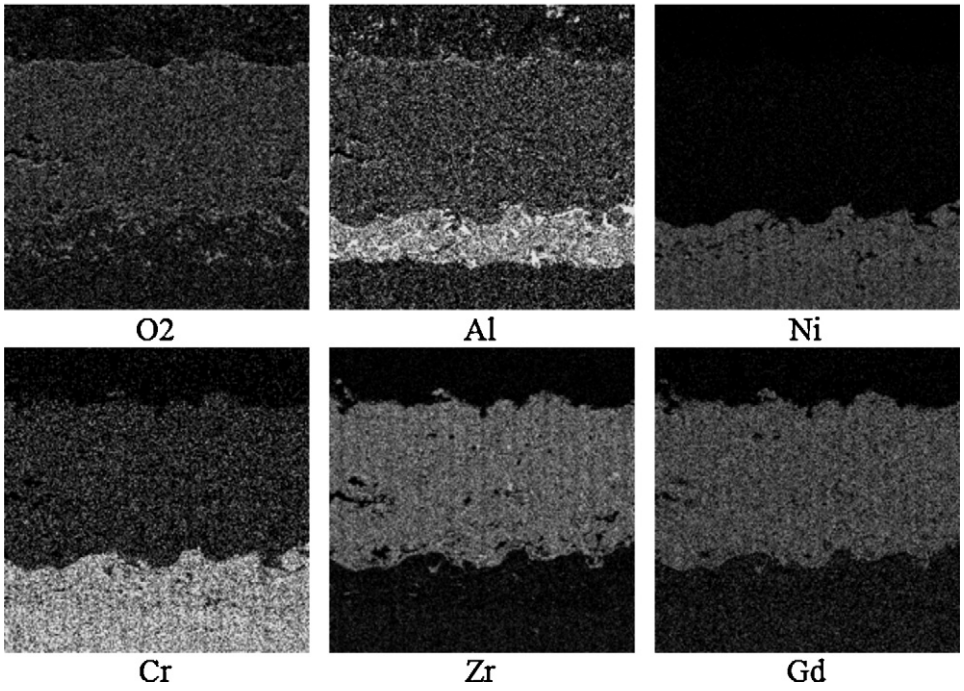

Fig. 8. Surface distribution of components in TBC $Gd_2Zr_2O_7$layer.

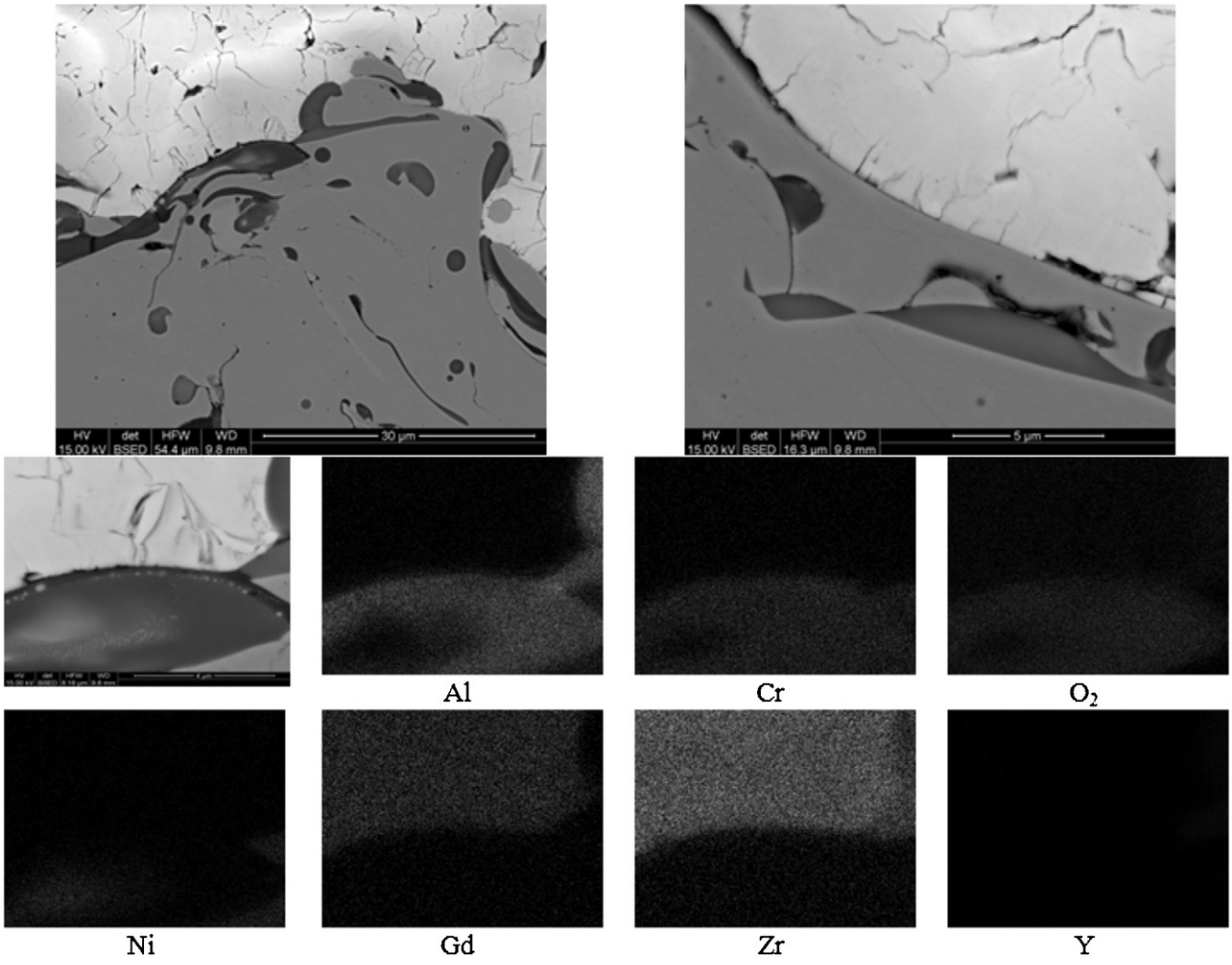

Fig. 9. Surface distribution of components in TBC $Gd_2Zr_2O_7$ layer in interface zone between a ceramic layer and the NiCrAlY prime layer.

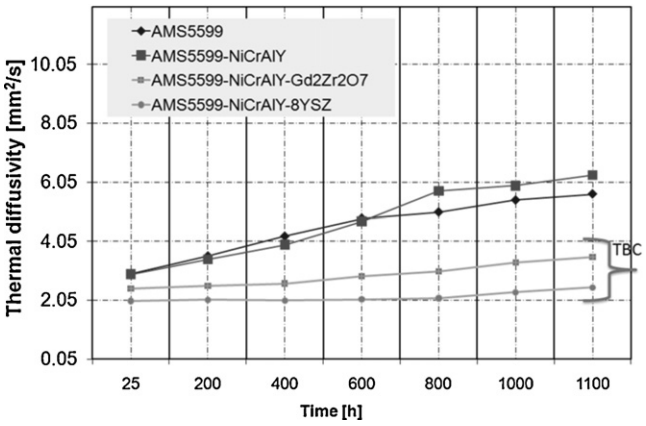

Fig. 10. Thermal diffusivity of TBC 8YSZ and $Gd_2Zr_2O_7$ layers, measured as a monolithic system.

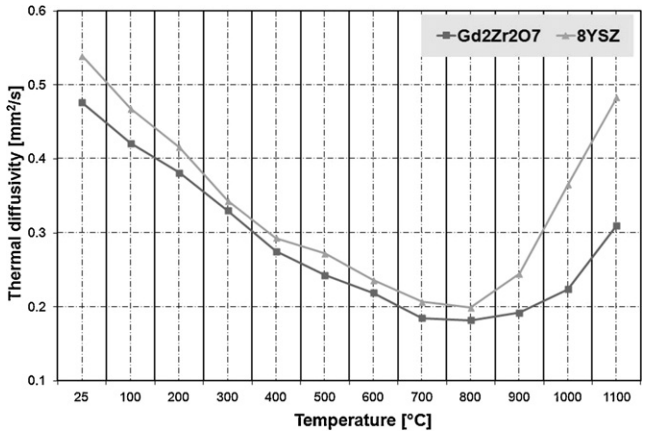

Fig. 11. Thermal diffusivity of ceramic top coat of 8YSZ and $Gd_2Zr_2O_7$ types obtained from two-layers model with contact resistance.

From the point of view of porosity of a ceramic layer, the reduction in thermal conductivity is mainly related to the volume participation of pores and their sizes. The thermal conductivity of gas contained in the pores of the TBC layers is close to that of free gases (approximately 0.025 W/mK for air), which indicates that the pore sizes are much bigger on average than the mean-free path of the gas molecules. If the pore sizes fall significantly below the gas mean-free path length, then the thermal conductivity drops below the typical value for free gases and becomes related exclusively with Knudsen's conductivity. Pore sizes (and grain sizes as well) are also meaningful from the point of view of radiative heat transport, because grain boundaries and similar microstructural elements can scatter the radiative heat-transfer component. Fine-grained structure and fine pores strongly scatter the heat stream and reduce emission of infrared radiation.[38]

Grain boundaries are another microstructural element that contribute to determining the thermal insulation properties of sprayed layers. The scattering of phonons from grain boundaries can lower thermal conductivity in the low-temperature range by reducing the phonon mean-free path in a sprayed layer. And this effect is stable, even at high temperatures.[39,40] As for phonon scattering from grain boundaries, the introduction of significant-size inclusions will further shorten the phonon mean-free path in the microstructure of a layer. In this case, the effect depends on the radius of the inclusion. This aspect was stated experimentally, and it was shown that that smaller inclusions and higher-volume participation of inclusions results in a noticeable drop in thermal conductivity.[39,40]

The thermal diffusivity of the materials analyzed is presented in Fig. 10. The curve for the AMS5599 alloy is typical for metal alloys, with the thermal diffusivity increasing with temperature. In this case, heat transport is dominated by the electron mechanism and the phonon mechanism is not significant. The thermal diffusivity curve for an alloy of the base material, with a sprayed NiCrAl layer, is similar. A stronger overall increase in diffusivity for a binary system can be seen and indicates the increased influence of the interlayer at higher temperature. Applying an outer ceramic $Gd_2Zr_2O_7$ layer type decreased the thermal diffusivity of the AMS5599-NiCrAlY binary system. At 1100 °C, the drop in diffusivity is almost a factor of two. To put the results in perspective, we also show the diffusivity of a conventional 8YSZ layer.

The lowest thermal diffusivity of the whole system is for a conventional coating based on the 8YSZ powder. However, these results are not authoritative, because they do not take into account the real thickness of the ceramic layers. To do so would require determining the thermal diffusivity of the ceramic layers via mathematical models, which would render the results independent of layer thickness. Thus, in addition to measured data, we used the PROTEUS package for this purpose. The thickness of the measured layers was 300 and 190 μm for the 8YSZ and $Gd_2Zr_2O_7$ coatings, respectively.

We applied a bilayer model to calculate the thermal diffusivity of the ceramic layers in both TBC systems. The base material plus bondcoat was treated as the base material and the outer ceramic layer was treated as an unknown material. The results, presented in Fig. 11, indicate a thermal diffusivity inversely proportional to temperature (typical for polycrystalline materials) over the range from ambient temperature to approximately 800 °C. At higher temperatures, the observed increase in thermal diffusivity to 1100 °C is attributed to radiative heat transport. It is clear that the $Gd_2Zr_2O_7$ coating is characterized by a lower thermal diffusivity, which we attribute to the properties of the charge material itself and to the microstructure of the deposited layer (porosity). However, the porosity results demonstrate that the thermal diffusivity of the $Gd_2Zr_2O_7$ layer is slightly larger (∼5%) than that of the TBC 8YSZ layer.

Based on the measurements of the thermal diffusivity of the layers and on the specific heat, density, and coefficient of linear extension, we calculated the coefficient of thermal diffusivity for the analyzed ceramic layers of feedstock powders[22–24] (Fig. 12).

The results of these calculations indicate a lower thermal diffusivity for the TBC layers, which were obtained from gadolinium–zirconate-based powders. This difference decreases slightly with increasing temperature, but the proposed layer is still characterized by a thermal diffusivity approximately 20% less than that of conventional layers.

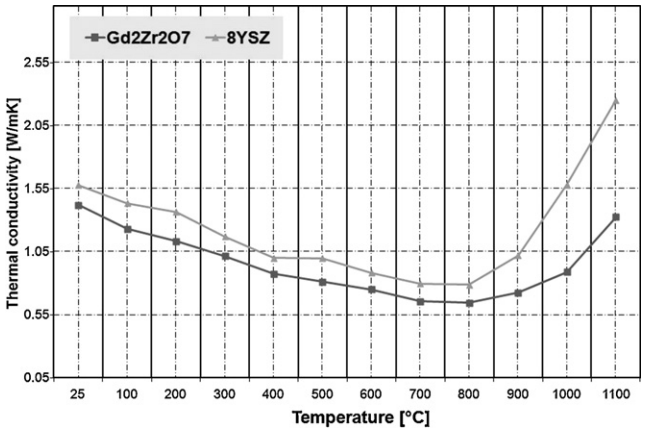

Fig. 12. Thermal conductivity of ceramic top coat of 8YSZ and $Gd_2Zr_2O_7$ types.

4. Conclusion

Our measurements revealed that using gadolinium–zirconate-based powder leads to a TBC coating characterized by significantly improved thermal insulation properties—at a significantly lower outer-ceramic-layer thickness—compared with conventional layers based on 8YSZ powders. In addition, the microstructure, inner structure, and geometrical parameters of the proposed layer based on $Gd_2Zr_2O_7$ powder (deposited with standard plasma-spraying parameters) are comparable to those of conventional layers.

Acknowledgments

We gratefully acknowledge the financial support of the Structural Funds in the Operational Program, Innovative Economy (IE OP) financed by the European Regional Development Fund, Project No. POIG.0101.02-00-015/09.

References

1. Miller RA. Thermal barrier coatings for aircraft engines: history and directions. *J Therm Spray Technol* 1997;**6**:35.
2. Clarke DR, Levi CG. Materials design for the next generation thermal barrier. *Coatings Annu Rev Mater Res* 2003;**33**:383.
3. Schulz U. Phase transformation in EB-PVD yttria partially stabilized zirconia TBCs during annealing. *J Am Ceram Soc* 2000;**83**:904.
4. Lughi V, Tolpygo VK, Clarke DR. Microstructural aspects of the sintering of TBCs. *Mat Sci Eng A – Struct* 2004;**368**:212.
5. Hutchinson RG, Fleck NA, Cocks ACF. A sintering model for thermal barrier coatings. *Acta Mater* 2006;**54**:1297.
6. Zhu D, Miller RA. Development of advanced low conductivity thermal barrier coatings. *J Therm Spray Technol* 2000;**9**:1759.
7. Jones RL. *Experiences in seeking stabilizers for zirconia having hot corrosion-resistance and high temperature tetragonal (t') stability*. Washington, DC: NRL/MR/6170-96-7841, Naval Research Laboratory; 1996.
8. Schulz U, Leyens C, Fritscher K, Peters M, Saruhan-Brings B, Lavigne O, et al. Some recent trends in research and technology of advanced TBCs. *Aerosp Sci Technol* 2003;**7**:73.
9. Zhu D, Miller RA. Thermal conductivity and sintering behavior of advanced TBCs. *Ceram Eng Sci Proc* 2002;**23**:457.
10. Cao XQ, Vassen R, Stoever D. Ceramic materials for thermal barrier coatings. *J Eur Ceram Soc* 2004;**24**:1.
11. Clarke DR, Phillpot SR. Thermal barrier coating materials. *Mat Today* 2005;**8**:22.
12. Pan W, Wan CL, Xu Q, Wang JD, Qu ZX. Thermal diffusivity of samarium–gadolinium. Zirconate solid solutions. *Thermochim Acta* 2007;**455**:16.
13. Lehmann H, Pitzer D, Pracht G, Vassen R, Stöver D. Thermal conductivity and thermal expansion coefficients of the lanthanum rare-earth-element zirconate system. *J Am Ceram Soc* 2003;**86**:1338.
14. Suresh G, Seenivasan G, Krishnaiah MV, Murti PS. Investigation of the thermal conductivity of selected compounds of lanthanum, samarium and europium. *J Alloys Compd* 1998;**269**:L9.
15. Suresh G, Seenivasan G, Krishnaiah MC, Srirama Murti P. Investigation of the thermal conductivity of selected compounds of gadolinium and lanthanum. *J Nucl Mater* 1997;**249**:259.
16. Wu J, Wei X, Padture NP, Klemens PG, Gell M, Garcia E, et al. Low-thermal-conductivity rare-earth zirconates for potential thermal-barrier-coating applications. *J Am Ceram Soc* 2002;**85**:3031.
17. Vassen R, Cao X, Tietz F, Basu D, Stoever D. Zirconates as new materials for thermal barrier coatings. *J Am Ceram Soc* 2000;**83**:2023.
18. Evans AG, Mumm DR, Hutchinson JW, Meier GH, Pettit FS. Mechanisms controlling the durability of thermal barrier coatings. *Prog Mater Sci* 2001;**46**:505.
19. Strangman TE. Thermal barrier coatings for turbine airfoils. *Thin Solid Films* 1985;**127**:93.
20. Lu TJ, Levi CG, Wadley HNG, Evans AG. *J Am Ceram Soc 2001* 2001;**84**:2937, 84:2937.
21. Moskal G. Microstructure and thermal diffusivity of RE zirconate powders for TBC system obtained by the APS method. In: Gaal DS, Gaal PS, editors. *Proceedings of the thirtieth international thermal conductivity conference, proceedings of the eighteenth international thermal expansion symposium*. Pittsburgh, PA, USA: DEStech Publications, Inc.; 2009. p. 451.
22. Moskal G. Characteristics of selected thermal properties of ceramic powders type RE2Zr2O7, IV scientific conference; modern technologies in surface engineering; Spała, 27–30.09.2010. *Inżynieria Materiałowa* 2010; **4**:1107.
23. Moskal G, Iwaniak A, Rozmysłowska-Grund A. Characterization of thermal properties of micro-sized ceramic powders for APS deposition of ceramic layers. *Key Eng Mater* 2011;**484**:152–7.
24. Moskal G, Dercz G. Effect of heat treatment on structure and phase transformation of rare earth (Gd) zirconate. *Solid State Phenom* 2010; **163**:157.
25. Bengtsson P, Persson C. Modelled and measured residual stresses in plasma sprayed thermal barrier coatings. *Surf Coat Technol* 1997;**92**:78.
26. Widjaja S, Limarga AM. Hon Yip T, Modeling of residual stresses in a plasma-sprayed zirconia/alumina functionally graded-thermal barrier coating. *Thin Solid Films* 2003;**434**:216.
27. Kuroda S, Clyne TW. The quenching stress in thermally sprayed coatings. *Thin Solid Films* 1991;**200**:49.
28. Teixeira V, Andritschky M, Fischer W, Buchkremer HP, Stover D. Analysis of residual stresses in thermal barrier coatings. *J Mater Process Technol* 1999;**92–93**:209.
29. Tanaka M, Hasegawa M, Dericioglu AF, Kagawa Y. Measurement of residual stress in air plasma-sprayed Y_2O_3–ZrO_2 thermal barrier coating system using micro-Raman spectroscopy. *Mater Sci Eng A – Struct* 2006; **419**:262.
30. Levit M, Grimberg I, Weiss B-Z. Residual micromicro- and macrostresses in the plasma-sprayed zirconia-based TBCs. *Mater Lett* 1994;**19**:48.
31. Scardi P, Leoni M, Bertamini L. Influence of phase stability on the residual stress in partially stabilized zirconia TBC produced by plasma spray. *Surf Coat Technol* 1995;**7**:6–77, 106.
32. Scardi P, Leoni M, Bertamini L. Residual stresses in plasma sprayed partially stabilized zirconia TBCs: influence of the deposition temperature. *Thin Solid Films* 1996;**278**:96.
33. Jordan DW, Faber KT. X-ray residual stress analysis of a ceramic thermal barrier coating undergoing thermal cycling. *Thin Solid Films* 1993;**235**:137.
34. Levit M, Grimberg I, Weiss BZ. Residual stresses in ceramic plasma-sprayed thermal barrier coatings: measurement and calculation. *Mater Sci Eng A – Struct* 1996;**206**:30.
35. Moskal G, Rzychoń T, Witala B, Rozmysłowska A, Dercz G. XRD residual stress characterization of air plasma sprayed RE-zirconates type

of ceramic coatings. In: *59th Denver X-Ray Conference 2–6 August*. 2010.
36. Ranjbar-Far M, Absi J, Mariaux G, Shahidi S. Effect of residual stresses and prediction of possible failure mechanisms on thermal barrier coating system by finite element method. *J Therm Spray Technol* 2010; **19**:1054.
37. Garcia E, Miranzo P, Soltani R, Coyle TW. Microstructure and thermal behavior of thermal barrier coatings. *J Therm Spray Technol* 2008; **17**:478.
38. Golosnoy IO, Cipitria A, Clyne TW. Heat transfer through plasma-sprayed thermal barrier coatings in gas turbines: a review of recent work. *J Therm Spray Technol* 2009;**18**:809.
39. Charvat FR, Kingery WD. Thermal conductivity: XIII, effect of microstructure on conductivity of single-phase ceramics. *J Am Ceram Soc* 1957;**40**:306–15.
40. Klemens PG. Thermal conductivity of zirconia. In: Wils KE, Dinwiddie RB, Graves RS, editors. *Thermal Conductivity 23*. Lancaster: Technomies Publishing Co.; 1996. p. 209–20.